








## Article

# Synthesis, Structure, and Properties of $\text{EuLnCuSe}_3$ (Ln = Nd, Sm, Gd, Er)

Oleg V. Andreev<sup>1</sup>, Victor V. Atuchin<sup>2,3,4</sup> , Alexander S. Aleksandrovsky<sup>5,6</sup> , Yuriy G. Denisenko<sup>7,\*</sup> , Boris A. Zakharov<sup>8,9</sup> , Alexander P. Tyutyunnik<sup>10</sup> , Navruzbeq N. Habibullayev<sup>1</sup> , Dmitriy A. Velikanov<sup>5</sup> , Dmitriy A. Ulybin<sup>1,9</sup> and Daniil D. Shpindyuk<sup>1</sup>

- <sup>1</sup> Institute of Chemistry, University of Tyumen, 625003 Tyumen, Russia; o.v.andreev@utmn.ru (O.V.A.); habibullayev\_navruzbeq@mail.ru (N.N.H.); d.a.ulybin@mail.ru (D.A.U.); d.d.shpindyuk@utmn.ru (D.D.S.)
- <sup>2</sup> Laboratory of Optical Materials and Structures, Institute of Semiconductor Physics, SB RAS, 630090 Novosibirsk, Russia; atuchin@isp.nsc.ru
- <sup>3</sup> Research and Development Department, Kemerovo State University, 650000 Kemerovo, Russia
- <sup>4</sup> Department of Industrial Machinery Design, Novosibirsk State Technical University, 630073 Novosibirsk, Russia
- <sup>5</sup> Kirensky Institute of Physics, Federal Research Center, KSC, SB RAS, 660036 Krasnoyarsk, Russia; aleksandrovsky@kirensky.ru (A.S.A.); dponal@gmail.com (D.A.V.)
- <sup>6</sup> Department of Photonics and Laser Technology, Siberian Federal University, 660036 Krasnoyarsk, Russia
- <sup>7</sup> Department of General and Special Chemistry, Industrial University of Tyumen, 625000 Tyumen, Russia
- <sup>8</sup> Borskov Institute of Catalysis, SB RAS, 630090 Novosibirsk, Russia; b.zakharov@yahoo.com
- <sup>9</sup> Laboratory of Molecular Design and Ecologically Safe Technologies, Novosibirsk State University, 630090 Novosibirsk, Russia
- <sup>10</sup> Institute of Solid State Chemistry, UB RAS, 620990 Ekaterinburg, Russia; tyutyunnik@ihim.uran.ru
- \* Correspondence: yu.g.denisenko@gmail.com



**Citation:** Andreev, O.V.; Atuchin, V.V.; Aleksandrovsky, A.S.; Denisenko, Y.G.; Zakharov, B.A.; Tyutyunnik, A.P.; Habibullayev, N.N.; Velikanov, D.A.; Ulybin, D.A.; Shpindyuk, D.D. Synthesis, Structure, and Properties of  $\text{EuLnCuSe}_3$  (Ln = Nd, Sm, Gd, Er). *Crystals* **2022**, *12*, 17. <https://doi.org/10.3390/cryst12010017>

Academic Editor: Ana M. Garcia-Deibe

Received: 30 November 2021

Accepted: 17 December 2021

Published: 23 December 2021

**Publisher's Note:** MDPI stays neutral with regard to jurisdictional claims in published maps and institutional affiliations.



**Copyright:** © 2021 by the authors. Licensee MDPI, Basel, Switzerland. This article is an open access article distributed under the terms and conditions of the Creative Commons Attribution (CC BY) license (<https://creativecommons.org/licenses/by/4.0/>).

**Abstract:**  $\text{EuLnCuSe}_3$  (Ln = Nd, Sm, Gd, Er), due to their complex composition, should be considered new materials with the ability to purposefully change the properties. Samples of the  $\text{EuLnCuSe}_3$  were prepared using Cu, rare earth metal, Se (99.99%) by the ampoule method. The samples were obtained by the crystallization from a melt and annealed at temperatures 1073 and 1273 K. The  $\text{EuErCuSe}_3$  crystal structure was established using the single-crystal particle.  $\text{EuErCuSe}_3$  crystallizes in the orthorhombic system, space group  $Cmcm$ ,  $\text{KCuZrS}_3$  structure type, with cell parameters  $a = 4.0555$  (3),  $b = 13.3570$  (9), and  $c = 10.4602$  (7) Å,  $V = 566.62$  (6) Å<sup>3</sup>. In structure  $\text{EuErCuSe}_3$ , erbium ions are coordinated by selenium ions in the octahedral polyhedron, copper ions are in the tetrahedral coordination, europium ions are between copper and erbium polyhedra layers and are coordinated by selenium ions as two-cap trigonal prisms. The optical band gap is 1.79 eV. At 4.7 K, a transition from the ferromagnetic state to the paramagnetic state was detected in  $\text{EuErCuSe}_3$ . At 85 and 293 K, the compound is in a paramagnetic state. According to XRPD data,  $\text{EuLnCuSe}_3$  (Ln = Nd, Sm, Gd) compounds have a  $Pnma$  orthorhombic space group of the  $\text{Eu}_2\text{CuS}_3$  structure type. For  $\text{EuSmCuSe}_3$ ,  $a = 10.75704$  (15) Å,  $b = 4.11120$  (5) Å,  $c = 13.37778$  (22) Å. In the series of  $\text{EuLnCuSe}_3$  compounds, the optical band gap increases 1.58 eV (Nd), 1.58 eV (Sm), 1.72 eV (Gd), 1.79 eV (Er), the microhardness of the 205 (Nd), 210 (Sm), 225 (Gd)  $235 \pm 4$  HV (Er) phases increases, and the thermal stability of the phases increases significantly. According to the measurement data of differential scanning calorimetry, the  $\text{EuNdCuSe}_3$  decomposes, according to the solid-phase reaction  $T = 1296$  K,  $\Delta H = 8.2 \pm 0.8$  kJ/mol.  $\text{EuSmCuSe}_3$  melts incongruently  $T = 1449$  K,  $\Delta H = 18.8 \pm 1.9$  kJ/mol. For the  $\text{EuGdCuSe}_3$ , two ( $T_{\alpha \leftrightarrow \beta} = 1494$  K,  $\Delta H_{\alpha \leftrightarrow \beta} = 14.8$  kJ/mol,  $T_{\beta \leftrightarrow \gamma} = 1530$  K,  $\Delta H_{\beta \leftrightarrow \gamma} = 4.8$  kJ/mol) and for  $\text{EuErCuSe}_3$  three polymorphic transitions ( $T_{\alpha \leftrightarrow \beta} = 1561$  K,  $\Delta H_{\alpha \leftrightarrow \beta} = 30.3$  kJ/mol,  $T_{\beta \leftrightarrow \gamma} = 1579$  K,  $\Delta H_{\beta \leftrightarrow \gamma} = 4.4$  kJ/mol, and  $T_{\gamma \leftrightarrow \delta} = 1600$  K,  $\Delta H_{\gamma \leftrightarrow \delta} = 10.1$  kJ/mol). The compounds melt incongruently at the temperature of 1588 K,  $\Delta H_{\text{melt}} = 17.9 \pm 1.8$  kJ/mol and 1664 K,  $\Delta H_{\text{melt}} = 25.6 \pm 2.5$  kJ/mol, respectively. Incongruent melting of the phases proceeds with the formation of a solid solution of  $\text{EuSe}$  and a liquid phase.

**Keywords:** rare earth elements; complex sulfides; chalcogenides; crystal structure; magnetic properties

## 1. Introduction

Starting with the works of James A. Ibers [1], compounds of general composition  $A^{II}Ln^{III}BX_3$ , where A is an alkaline earth metal or europium, Ln is an element of the 4f subgroup, B is copper or silver, and X is a chalcogen, increasingly attract researcher's attention [2–5]. The presence of 3d, 4f elements in the composition of quaternary compounds makes them promising materials in the field of catalysis [6,7], nonlinear optics [8–14], and thermoelectricity [15].  $EuLnCuS_3$  exhibit ferro- and ferrimagnetic transitions at temperatures 4.5–5.4 K [16]. The compounds belong to semiconductors and have a band gap of 1.63–2.61 eV, according to the UV spectroscopy data [3,17].

In the  $A^{II}Ln^{III}BX_3$  family, the formation of more than 200 complex chalcogenide compounds was predicted. More than 100 sulfide compounds were synthesized and investigated, and only 23 selenide compounds are known [8,18–20].  $ALnCuSe_3$  crystallized in the following structural types (ST):  $SrLuCuSe_3$  type  $KCuZrS_3$  *Cmcm* [21],  $SrGdCuSe_3$ , type  $Eu_2CuS_3$  *Pnma*,  $SrLaCuSe_3$  type  $Ba_2MnS_3$  [20] *Pnma*,  $SrCeCuSe_3$  type  $Ba_2MnS_3$  [20],  $PbLuCuSe_3$   $PbTmCuSe_3$   $PbErCuSe_3$   $PbHoCuSe_3$   $PbDyCuSe_3$   $PbTbCuSe_3$ ,  $PbGdCuSe_3$  type  $Eu_2CuS_3$  *Pnma* [3].

Complex sulfides  $EuLnCuS_3$  crystallize in ST  $Ba_2MnS_3$  SG *Pnma* (Nd), ST  $KZrCuS_3$  SG *Cmcm* (Sm, Gd, Er). The optical band gap of  $EuErCuS_3$  is 1.934 eV [22]. Ferromagnets are  $EuNdCuS_3$  and  $EuSmCuS_3$  with magnetic phase transition temperatures of 3.1 K and 3.1 K, respectively [23]. Ferrimagnets are  $EuGdCuS_3$  ( $T_c = 5.2$  K) [16] and  $EuErCuS_3$  ( $T_c = 4.8$  K) [22]. Above the temperatures of magnetic transitions, the compounds exhibit paramagnetic properties [16,23].  $EuLnCuS_3$  exhibit polymorphism (Sm, Gd, Er), melt incongruently at temperatures of 1470 K (Nd), 1574 K (Sm), 1720 K (Gd), and 1735 K (Er). Data on the structure and properties of  $EuLnCuSe_3$  were not found in the literature.

For the synthesis of  $EuLnCuSe_3$ , rare earth elements were selected, which represent four tetrads of lanthanides, which would make it possible to trace the main regularities in the structure and properties of the compounds. Nd is in the first tetrad (La–Nd), Sm and Gd in the second tetrad (Sm–Gd), Gd simultaneously represents the third tetrad (Gd–Ho), and Er from the fourth tetrad (Er–Lu).

It is valuable to observe the structural parameters of several simple selenides related to the present study. The  $EuSe$  has a cubic NaCl-type structure, space group (SG) *Fm $\bar{3}m$* ,  $a = 6.185$  Å [24], and melts congruently at 2488 K [25]. The  $Nd_2Se_3$  compound has a cubic structure, ST  $Th_3P_4$   $a = 8.871$  Å.  $Sm_2Se_3$ ,  $Gd_2Se_3$  exist in the form of low-temperature modifications of the rhombic form  $\alpha$ - $La_2S_3$  and high-temperature modifications of the  $Th_3P_4$  type,  $a = 8.785$  Å,  $a = 8.718$  Å.  $Er_2Se_3$  crystallized in SG *Fddd*, ST  $Sc_2S_3$ ,  $a = 8.085$ ,  $b = 11.346$  and  $c = 24.140$  Å [26] All compounds melt congruently at temperatures  $T(Nd_2Se_3) = 2200$  K,  $T(Sm_2Se_3) = 2150 \pm 40$  K [27],  $T(Gd_2Se_3) = 1943$  K [28]  $T(Er_2Se_3) = 1520$  K [29].

As known, copper semi-selenide forms a solid solution region, described by the formula  $Cu_{2-x}Se$  [30,31]. The  $Cu_{1.999}Se$  composition was chosen as the initial one, due to the precipitation of copper during the synthesis of the  $Cu_2Se$  composition [30].  $Cu_2Se$  can exist in two polymorphic modifications:  $\alpha$ - $Cu_2Se$ , monoclinic system,  $a = 14.083$ ,  $b = 20.481$  and  $c = 4.145$  Å,  $\beta = 90.4^\circ$ , SG *P2<sub>1</sub>/n* [32] and  $\beta$ - $Cu_2Se$ , cubic system,  $a = 5.765$  Å, SG *F4 $\bar{3}m$*  [32]. The  $\alpha$ - $Cu_2Se \rightarrow \beta$ - $Cu_2Se$  phase transition occurs at a temperature of  $396 \pm 15$  K. The  $Cu_{2-x}Se$  phase melts congruently at 1403 K [33].

The aim of the article is to synthesize  $EuLnCuSe_3$ , to establish the structure, regularities in changes in crystal chemical parameters, optical band gap, thermal characteristics of compounds, and magnetic properties (Er).

## 2. Methods and Materials

### 2.1. Synthesis

Four types of samples of the  $EuLnCuSe_3$  compound were obtained: polycrystalline ingots, powder, single crystal, and technical ceramics.

The following simple substances were used as starting reagents: Cu 99.99 at. % (OJSC «Uralredmet», Sverdlovsk, Russia), Se 99.99 at. % (JSC «Khimreaktiv», Yekaterinburg,

Russia), and rare earth metals 99.99 at. % (TOPLUS, LTD, Guangzhou, China). Metal surfaces have been thoroughly brushed. The Cu plate was broken into pieces of 0.1–0.5 g. Each rare earth metal is ground with its own DeWALT DT5048 HSS-G steel drill. The surface condition of the drills did not change during the grinding process. The chip thickness was 2–10 microns. The Eu metal fibers have been mechanically separated. To reduce oxidation, metals are stored and crushed in an argon atmosphere. Weighed portions were taken, with an accuracy of 0.0001 g, on a METLER TOLEDO ME 204 balance. The stoichiometric batch weight was 5 g. Three parallel syntheses were performed. The mixture of metals was placed in a graphite crucible, with an inner diameter of 13 mm and a height of 35 mm, located in a quartz ampoule. Then, the ampoule was evacuated to a residual pressure of 0.1 Pa and sealed. The ampoules were placed in a muffle and heated from 473 to 1273 K, at a rate of 50 K per day. Then, the ampoules were kept at 1273 K for 50 h. The samples were melted in a high-frequency conversion unit. It was heated by increasing the power supplied to the inductor to the temperature at which the sample passed into the melt. The melting point was well established by visual inspection.

The samples crystallized from the melt had the shape of a cylinder, with a dense grain structure. Each of the samples is divided into two parts, which are placed in quartz ampoules; the ampoules are vacuumized and sealed.

Two series of annealed samples were obtained. At 1273 K, the samples were annealed for 50 h, at 1073 K for 500 h.

Powders of  $\text{EuErCuSe}_3$  were obtained by grinding annealed samples in an agate mortar to particles with a linear size of 1–100 microns.

Monocrystal of  $\text{EuErCuSe}_3$  with linear dimensions from 0.08 to 0.10 mm was picked out with a scalpel from a sample drained at 1070 K to study the crystal structure.

Technical ceramics of  $\text{EuErCuSe}_3$  were obtained for measuring the magnetic properties. The compound powder was pressed into a cylinder, with a diameter of 4 mm and height of 4 mm, under standard conditions in a cylindrical mold with a punch pressure of 0.8 tons. The mold is made of steel C80W1, the punch and matrix have mirror surfaces. There is no interaction between the matrix and substance to be pressed. The cylinder of the joint was placed in a quartz ampoule, which was evacuated and sealed. After annealing at 1073 K for 500 h, the sample acquired the necessary mechanical properties for the manufacture of a cylinder of the sample with parallel planes.

Impurity phases.

It was found that the impurity oxide phases  $\text{Er}_2\text{O}_3$  and  $\text{EuO}$ , contained on the surface of metal particles during heat treatment, form  $\text{Er}_2\text{O}_2\text{Se}$  and  $\text{Er}_2\text{Si}_2\text{O}_7$ . There is a clear relationship between the content of oxide phases in the starting materials and impurities in the samples after synthesis. According to the XRD data and microstructure analysis,  $\text{EuErCuSe}_3$  contained of 1.9 mass (m.) %  $\text{Er}_2\text{O}_2\text{Se}$  (ICDD PDF Entry No 01-074-0352) [34], of 4.1 m. %  $\text{Er}_2\text{Si}_2\text{O}_7$  (01-073-3003) [35].

The samples of  $\text{EuLnCuSe}_3$ , after annealing, contained the following impurity phases:  $\text{EuNdCuSe}_3$ : 8.4 m. %  $\text{NdCuSeO}$  (ICDD PDF Entry No. 00-046-0437) [36], 3.3 m. %  $\text{EuNdSe}_2$ , 0.9 m. %  $\text{EuNd}_2\text{Se}_4$  (01-077-7873) [37],  $\text{EuSmCuSe}_3$ : 7.4 m. %  $\text{SmCuSeO}$  (00-051-0065, 01-082-1480) [38], 1.4 m. %  $\text{EuSmSe}_2$  (01-075-6214, 03-065-4615) [39], 0.9 m. %  $\text{EuSm}_2\text{Se}_4$  (01-077-7899) [37],  $\text{EuGdCuSe}_3$ : 3.1 m. %  $\text{GdCuSeO}$  (00-051-0068; 01-085-2207) [40], and 1.9 m. %  $\text{EuGdSe}_2$ .

## 2.2. Analysis Methods

The X-ray powder diffraction (XRPD) patterns of samples, obtained by crystallization from the melt and annealed at 1073 K (XRPD), were collected at room temperature on a STADI-P (STOE) diffractometer in the transmission geometry, with a linear mini-PSD detector, using  $\text{CuK}\alpha_1$  radiation in the  $2\theta$  range from 5 to  $120^\circ$ , with the step of  $0.02^\circ$ . Polycrystalline silicon ( $a = 5.43075(5) \text{ \AA}$ ) was used as an external standard. Possible impurity phases were checked by comparing X-ray diffraction (XRPD) patterns with those given in the PDF2 database (ICDD, USA, release 2016). The crystal structure refinement

was carried out with the GSAS program suite, using XRPD data [41,42]. The peak profiles were fitted with a pseudo-Voigt function,  $I(2\theta) = x \times L(2\theta) + (1 - x) \times G(2\theta)$  (where L and G are the Lorentzian and Gaussian parts, respectively). The peak width angular dependence was described by the relation  $(FWHM)^2 = Utg^2\theta + Vtg\theta + W$ . The background level was described by a combination of 36-order Chebyshev polynomials. The absorption correction function for a flat plate sample in the transmission geometry was applied.

A single-crystal XRD study of EuErCuSe<sub>3</sub> was performed, using a STOE IPDS II diffractometer with MoK $\alpha$  radiation and an image-plate detector. A sample, with dimensions of 0.08–0.10 mm, was isolated from a sample annealed at 1273 K. The parameters, characterizing the data collection and crystal structure refinement, are summarized in Table 1. X-AREA [43] was used for the data collection and CrysAlis Pro [44], for data reduction and cell refinement. The crystal structure was solved with SHELXT [45] and refined using SHELXL-2018 [46] with ShelXle as a GUI [47]. The atomic parameters for all atoms were refined in the anisotropic approximation. Further details of the crystal structure investigations may be obtained from the joint CCDC/FIZ Karlsruhe online deposition service [48] <https://www.ccdc.cam.ac.uk/structures/> by quoting the deposition number CSD 2122151 (accessed on 20 October 2021).

**Table 1.** Main parameters of data collection and crystal structure refinement.

Crystal Data	
Chemical Formula	EuErCuSe <sub>3</sub>
$M_r$	619.64
Crystal system, space group	Orthorhombic, <i>Cmcm</i>
Temperature (K)	298
$a, b, c$ (Å)	4.0555 (3), 13.3570 (9), 10.4602 (7)
$V$ (Å <sup>3</sup> )	566.62 (6)
$Z$	4
Radiation type	Mo $K\alpha$
No. of reflections for cell measurement	863
$\mu$ (mm <sup>-1</sup> )	48.44
Crystal size (mm) and shape	0.10 × 0.08 × 0.03, block
Data Collection	
Absorption correction	Multi-scan ( <i>CrysAlis PRO</i> 1.171.40.53)
$T_{min}, T_{max}$	0.047, 0.068
No. of measured, independent and observed ( $I > 2\sigma(I)$ ) reflections	1336, 313, 270
$R_{int}$	0.080
$(\sin \theta / \lambda)_{max}$ (Å <sup>-1</sup> )	0.602
Range of $h, k, l$	$h = -4 \rightarrow 4, k = -12 \rightarrow 16, l = -12 \rightarrow 12$
Refinement	
$R(F^2 > 2\sigma(F^2)), wR(F^2), S$	0.031, 0.070, 1.05
No. of reflections	313
No. of parameters	24
$\Delta_{max}, \Delta_{min}$ (e Å <sup>-3</sup> )	1.78, -2.08

The particle micromorphology and contents of chemical elements in samples was studied by scanning electron microscopy (SEM) Tescan Mira 3 LMU (Brno, Czech Republic). Microhardness was measured on an Shimadzu HVM-G21DT microhardness tester, at the

load of 490.3 mN (50 g), using the HMV-G instrument software (Kyoto, Japan), and it was measured on a polycrystalline sample. Reflection spectra were recorded on a Shimadzu UV-3600 spectrophotometer (Kyoto, Japan). The studied sample was in the powder form. The studies were carried out on samples annealed at 1073 K.

Magnetic measurements were performed on a polycrystalline ceramic  $\text{EuErCuSe}_3$  sample, shaped as a cylinder of 4 mm in diameter and 4 mm high. The sample mass  $M$  was 0.2888 g. To impart a mechanical strength to the sample, it was preliminarily pressed and annealed in an oven at the temperature of 1070 K for 250 h. The magnetic field dependences of the magnetic moment  $m$  of the sample, in the range of magnetic fields  $H = 0\text{--}\pm 15$  kOe and temperature range from liquid nitrogen to room temperature, were recorded on a vibrating sample magnetometer [49] with an electromagnet, designed by I.M. Puzey [50]. The study of the  $\text{EuErCuSe}_3$  magnetic susceptibility in weak magnetic fields, in the temperature range from liquid helium to room temperature, was carried out with the use of an original SQUID (superconducting quantum interference device) magnetometer [51,52]. The temperature dependences of the sample magnetic moment  $m$  were measured in two modes: (1) during cooling, in the absence of magnetic field (ZFC—zero-field cooling), and (2) when cooling in a magnetic field (FC—cooling in a nonzero magnetic field).

Thermal analysis was performed on two independent units. The NETZSCH Jupiter STA 449 F3 device is equipped with a W-3% Re-W-25% Re thermocouple. A sample obtained by crystallization from a melt and annealed at 1073 K was used. A cylinder weighing 70–110 mg was cut out of the sample. The sample adhered tightly to the walls of a conical graphite crucible, with the volume of 0.1 mL, grade G-8. The survey was carried out in a helium atmosphere (99.99999 at. % Cryogen Russia). The results were processed using the Proteus analysis software [53]. The thermal analysis on a SETARAM SETSYS Evolution device, a PtRh-6%–PtRh-30%. A powder sample, weighing  $\text{EuErCuSe}_3$  100 mg, was taken from the same  $\text{EuErCuSe}_3$  sample. The compound crystals were placed in a quartz conical ampoule, evacuated, and sealed. The ampoule had a flat bottom, and the ampoule volume was 0.1 mL. The DSC results were processed using the SETSOFT 2000 program.

### 3. Results and Discussion

As shown in Figure 1, the  $\text{EuErCuSe}_3$  samples were obtained by the crystallization from a melt (Figure 1b), as a powder (Figure 1c), and technical ceramics (Figure 1d). The phase compositions of the samples, obtained in the parallel synthesis, were qualitatively similar. The samples contained more than 94 mass %  $\text{EuErCuSe}_3$ , and the representative (XRPD) pattern is shown in Figure 1a (the sample annealed at 1073 K). The XRPD pattern of  $\text{EuErCuSe}_3$  was fitted using the starting model, obtained from the single-crystal structure determination given below, and the results are in perfect agreement for both cell parameters and atom coordinates (See ESI). The diffractometry data of the  $\text{EuErCuSe}_3$  compound are identified in the orthorhombic system SG  $Cmcm$ .

The crystal structure of  $\text{EuErCuSe}_3$  is shown in Figure 2, and it is very similar to that of  $\text{EuErCuS}_3$  [22], despite that the compounds belong to different structural types. The  $\text{EuErCuSe}_3$  crystal structure can be described as the layers parallel to the (010) crystallographic plane. Each layer is built of  $\text{ErSe}_6$  octahedra and  $\text{CuSe}_4$  tetrahedra. Eu cations are located between these layers. The atom coordinates determined for the  $\text{EuErCuSe}_3$  structure are presented in Table S1 (Supplementary Materials). The bond lengths and angles are summarized in Table S2 (Supplementary Materials). An increase in the metal-chalcogen bond lengths correlate with an increase in the ionic radius of selenium ion  $r\text{Se}^{2-} = 1.98$  Å, as compared to that of the sulphur ion  $r\text{S}^{2-} = 1.84$  Å [54]. The unit cell parameters of  $\text{EuErCuSe}_3$  (Table 1) increase proportionally, in comparison with  $\text{EuErCuS}_3$   $a = 10.1005(2)$  Å,  $b = 3.91255(4)$  Å,  $c = 12.8480(2)$  Å;  $V = 507.737(14)$  Å<sup>3</sup>,  $Z = 4$ , and  $\rho_x = 6.266$  g/cm<sup>3</sup> [22]. Complete structural data were deposited via the joint CCDC/FIZ Karlsruhe deposition service, with refcode CSD 2122151. In the series of  $\text{EuLnCuSe}_3$  compounds, the structural type changes, in proportion to a decrease in the ionic radii of rare earth elements  $r\text{Nd}^{3+}$

(coordination number = 6) = 0.983 Å,  $r_{\text{Sm}^{3+}} = 0.958$  Å,  $r_{\text{Gd}^{3+}} = 0.938$  Å [55], the values of the unit cell parameters monotonically decrease (Figure 3, Table 2).

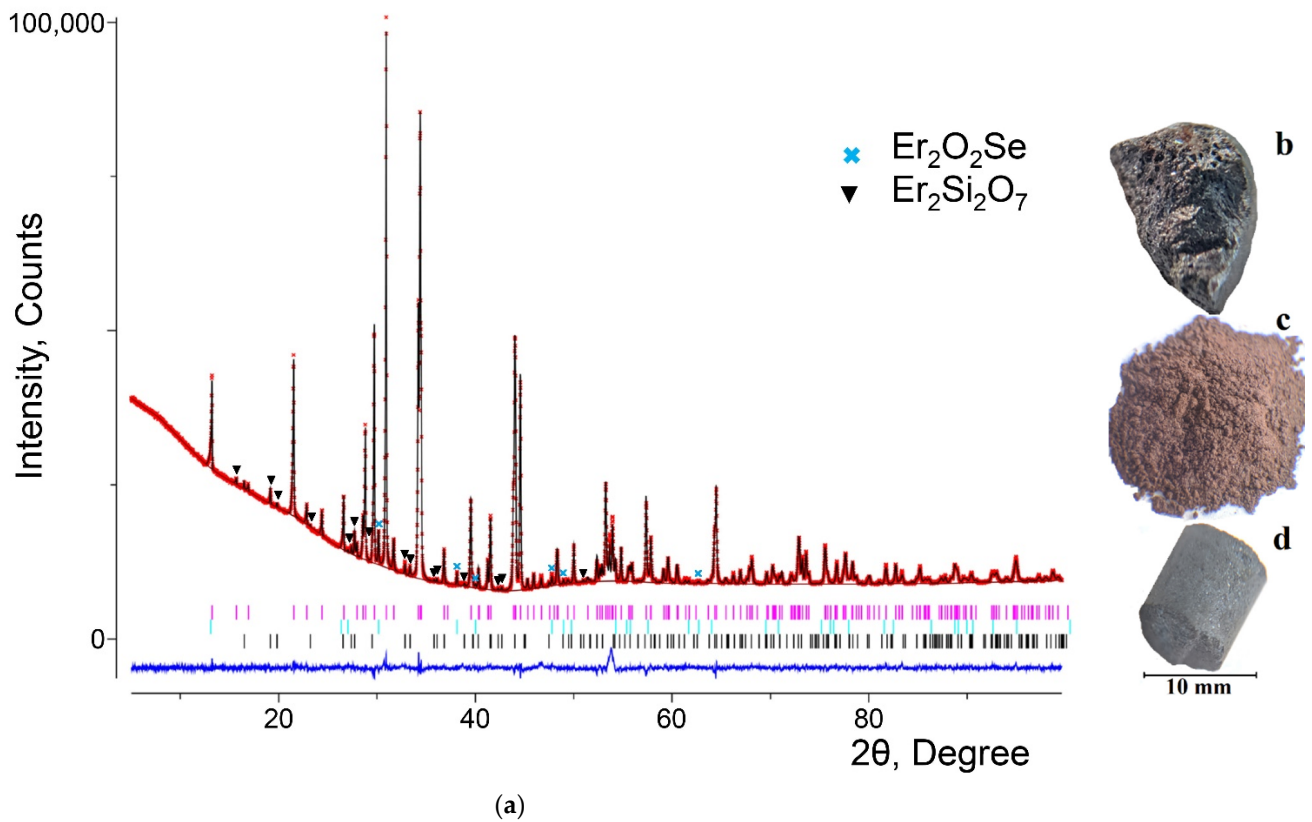


**Figure 1.** XRPD pattern (a) and photographs of  $\text{EuErCuSe}_3$  samples, (b)—a sample obtained by the crystallization from a melt, (c)—powder, (d)—technical ceramics. Magenta, blue, and black vertical marks correspond to the positions of the Bragg reflections for  $\text{EuErCuSe}_3$ ,  $\text{Er}_2\text{O}_2\text{Se}$ , and  $\text{Er}_2\text{Si}_2\text{O}_7$ , respectively.

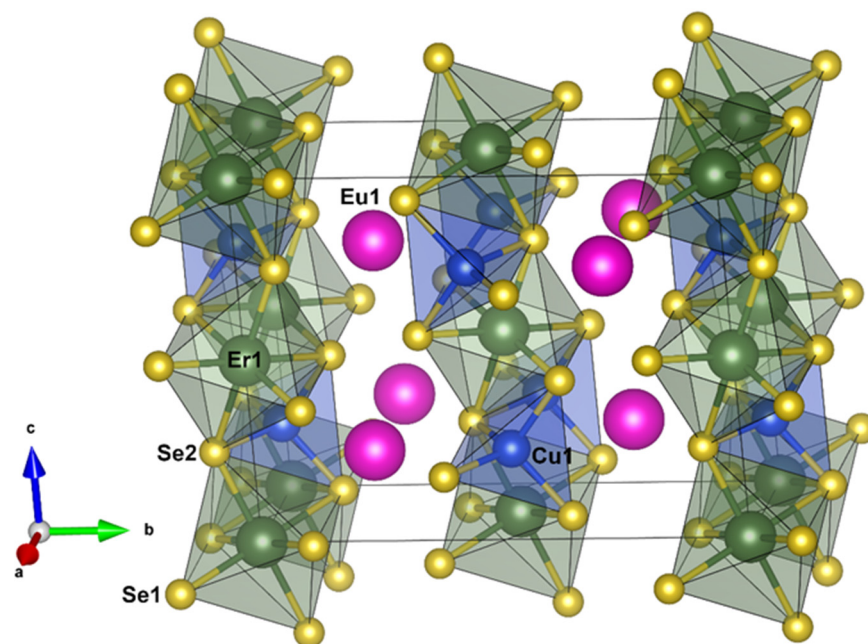


**Figure 2.** Crystal structure of  $\text{EuErCuSe}_3$ .

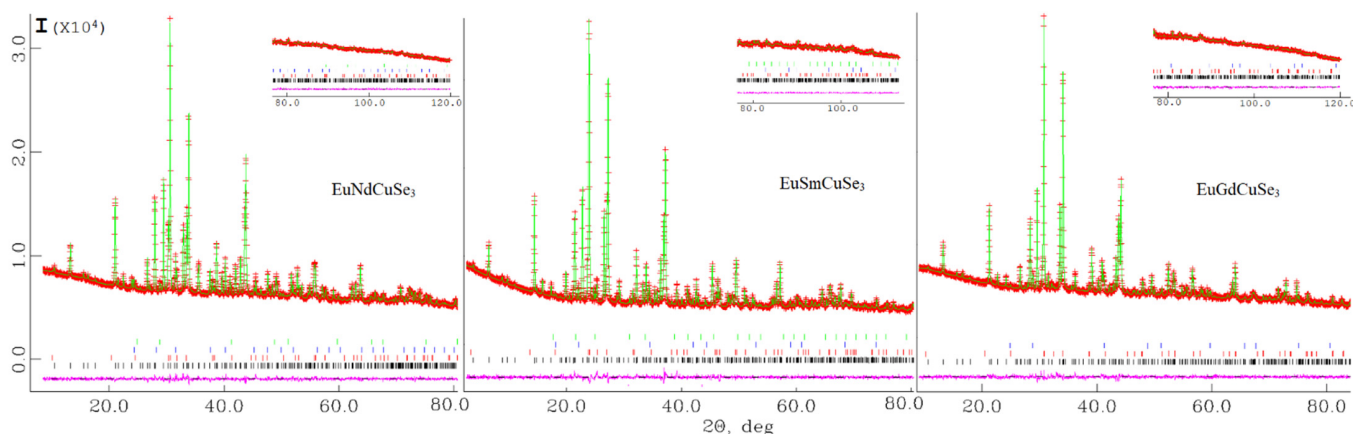


**Figure 3.** XRPD patterns of  $\text{EuLnCuSe}_3$  compounds (the sample annealed at 1073 K).

**Table 2.** Unit cell parameters of  $\text{EuLnCuSe}_3$  compounds (the sample annealed at 1073 K).

Ln	Nd	Sm	Gd
Space group	<i>Pnma</i>	<i>Pnma</i>	<i>Pnma</i>
Structure type	$\text{Eu}_2\text{CuSe}_3$ ( $\text{Gd}_3\text{NiSi}_2$ )	$\text{Eu}_2\text{CuSe}_3$ ( $\text{Gd}_3\text{NiSi}_2$ )	$\text{Eu}_2\text{CuSe}_3$ ( $\text{Gd}_3\text{NiSi}_2$ )
<i>a</i> , Å	10.87487 (18)	10.75704 (15)	10.67493 (22)
<i>b</i> , Å	4.13258 (6)	4.11120 (5)	4.09671 (7)
<i>c</i> , Å	13.36404 (22)	13.37778 (22)	13.39231 (31)
<i>V</i> , Å <sup>3</sup>	600.597 (16)	591.624 (14)	585.673 (21)
$\rho_{\text{xrd}}$ , gm/cm <sup>3</sup>	6.589	6.767	6.914
Z	4	4	4

The  $\text{EuErCuSe}_3$  sample was obtained by sintering ground metal selenides at 1073 K for 500 h. As seen in Figure 4, the  $\text{EuErCuSe}_3$  phase crystals are predominantly oval with faceting elements. The average grain size is 5–30  $\mu\text{m}$ . In some grains, the layered structure is clearly traced (Figure 4a). At individual points of the sintered powder, there are  $\text{Er}_2\text{O}_2\text{Se}$  grains, in which the oxygen content is detected (Figure 4b). A thin section was prepared from the cast annealed sample of  $\text{EuErCuSe}_3$ . According to the SEM data, chemical elements are evenly distributed in the sample (Figure 4c, Table 3). The constituent element ratio, within the limits of determination errors, is consistent with the nominal composition of the sample.

Several tens of imprints of a Vickers diamond indenter were obtained on a thin section of a polycrystalline sample of  $\text{EuLnCuSe}_3$ . The regular geometric imprints without cracks, or with one limited crack, were selected. The  $\text{EuLnCuSe}_3$  polycrystal microhardness was determined as  $H = 205$  (Nd),  $H = 210$  (Sm),  $H = 225$  (Gd)  $H = 235 \pm 4$  HV (Er),  $235 \pm 4$  HV.

The reflection spectra were recorded in the range of 200–1400 nm. The corresponding Kubelka–Munk function for  $\text{EuErCuSe}_3$  is shown in Figure 5, in comparison to the recently studied orthorhombic crystal  $\text{EuErCuS}_3$  [22]. The bandgap of the latter is equal to 1.94 eV, and it was explained [22] by the presence of 5d electronic states of the  $\text{Eu}^{2+}$  ion at the conduction band bottom. The  $\text{EuErCuSe}_3$  bandgap is a bit narrower, and it is equal to 1.79 eV.  $\text{EuErCuSe}_3$  crystallizes in the space group different from that of  $\text{EuErCuS}_3$ . However, both crystal structures belong to the same orthorhombic symmetry class. Therefore, the  $\text{EuErCuSe}_3$  bandgap narrowing, with respect to that of  $\text{EuErCuS}_3$ , could be ascribed mainly to the lower position of the subbands originating from the 5d states of the  $\text{Eu}^{2+}$  ion in the field of Se ion potential. An increase in the ionic radius of  $\text{Ln}^{3+}$  for elements of the beginning of the series further lowers the position of the 5d level, which causes a decrease in the bandgap of compounds:  $\text{EuNdCuSe}_3$  1.58 eV,  $\text{EuSmCuSe}_3$  1.58 eV, and  $\text{EuGdCuSe}_3$

1.72 eV. However, it should be noted that the behavior of the Kubelka–Munk function, for all complex selenenides in the regions below the values of the bandgap, is very peculiar.

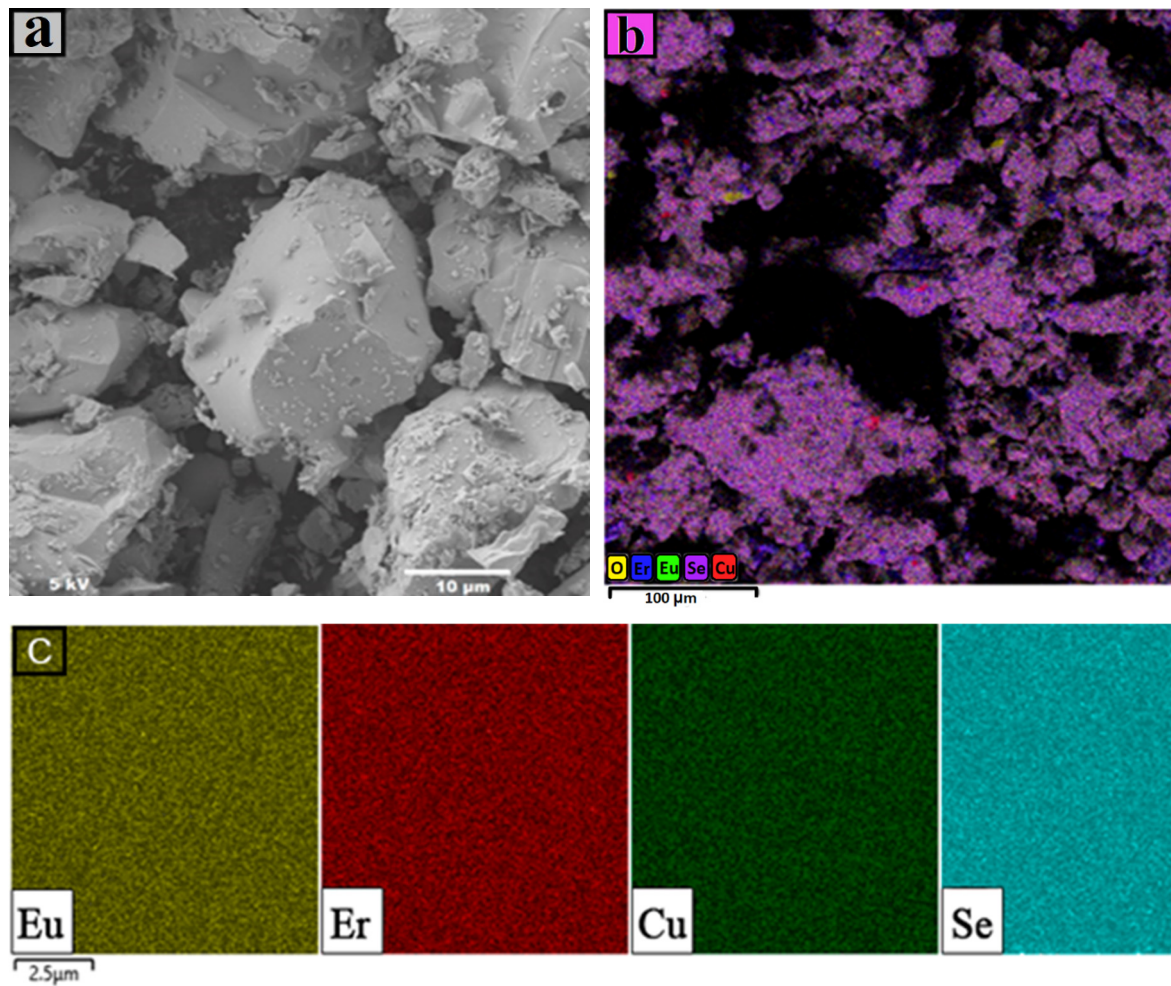


**Figure 4.** SEM patterns of  $\text{EuErCuSe}_3$  particles (a), element mapping in the sintered  $\text{EuErCuSe}_3$  powder (b), and constituent element maps (c), recorded in the polished  $\text{EuErCuSe}_3$  sample, annealed at 1073 K.

**Table 3.** Theoretical (B) and experimental (C) (according to the SEM data) contents of chemical elements in the  $\text{EuErCuSe}_3$  samples.

Element	Theoretical Content Mass. %	Sample B Mass. %	Sample C Mass. %
Eu	24.5	25.3	$25.3 \pm 0.3$
Er	27.0	27.5	$26.4 \pm 0.3$
Cu	10.3	10.3	$10.4 \pm 0.3$
Se	38.2	36.9	$37.9 \pm 0.3$

While, in the case of  $\text{EuErCuS}_3$ , the behavior close to that typical for Urbach tail is observed below 1.94 eV; in the case of  $\text{EuErCuSe}_3$ , something like the formation of the additional narrower bandgap, with a width below 1 eV, can be suspected.

This second bandgap may correspond to additional bands originating from the main composition of the material and positioned within the main bandgap or to the crystal structure, possibly a complex effect, including impurities. A further study with the help of ab initio simulations is desirable.



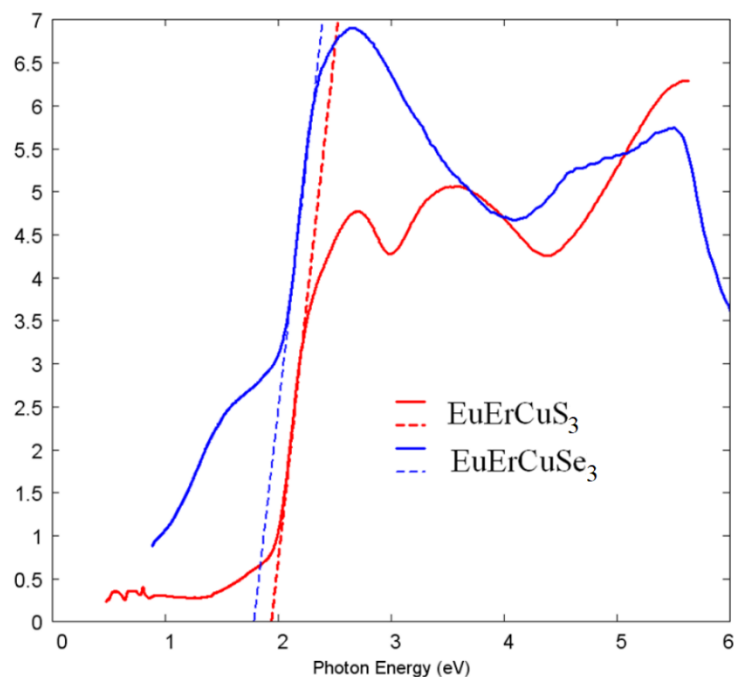


**Figure 5.** Kubelka–Munk functions and bandgaps for EuErCuSe<sub>3</sub> (blue,  $E_g = 1.79$  eV) and EuErCuS<sub>3</sub> (red,  $E_g = 1.94$  eV), the sample annealed at 1073 K.

At temperatures 293 and 85 K, the EuErCuSe<sub>3</sub> mass magnetization:

$$\sigma = m/M$$

is directly proportional to the strength of magnetic field  $H$  (Figure 6a), which indicates that the substance is in a paramagnetic state.

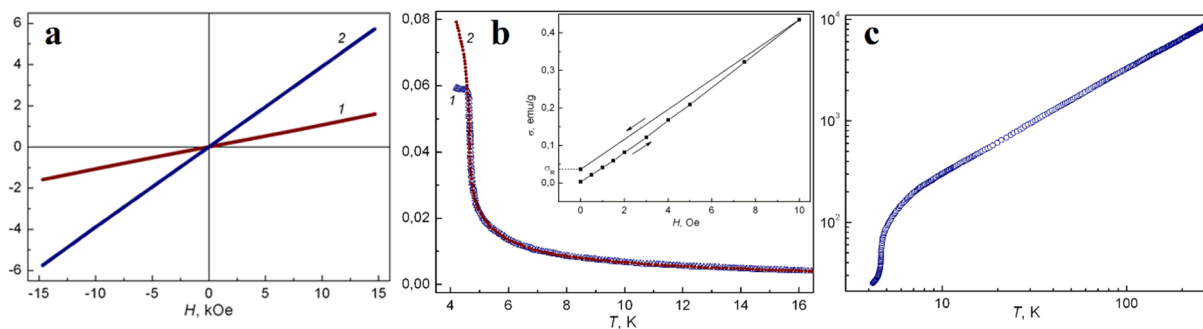


**Figure 6.** Experimental magnetic curves for the EuErCuSe<sub>3</sub> sample. (a) Magnetic field dependences of the magnetization, at temperatures 293 K (1) and 85 K (2). (b) Temperature dependences of the magnetization, recorded in the ZFC (1) and FC (2) modes.  $H = 2$  Oe. The inset shows a fragment of a particular hysteresis loop at  $T = 4.2$  K. (c) Temperature dependence of the inverse magnetic susceptibility.  $H = 10$  Oe.

At a temperature of several kelvin, a magnetically-ordered state is realized in the substance under study. There is a difference in the temperature dependences of the magnetizations  $\sigma(T)$ , taken in the ZFC and FC modes (see Figure 6b). The sample has a remanent magnetization  $\sigma_R$  at  $T = 4.2$  K (see inset in Figure 6b). The temperature of the magnetic phase transition is  $T_c = 4.7$  K. The temperature dependence of the inverse magnetic susceptibility (Figure 6c) is typical for magnets with a ferrimagnetic type of ordering [52].

$$1/\chi = H/\sigma$$

At high temperatures, the magnetic susceptibility  $\chi$  obeys the Curie-Weiss law. The dependence  $1/\chi(T)$  is linear:

$$\chi(T) = \frac{C}{T - \Theta},$$

where  $C$  and  $\Theta$  are constants. With decreasing temperature, the inverse magnetic susceptibility  $1/\chi$  is decreased steeply, tending to zero, as  $T \rightarrow T_c$ . Linear extrapolation of the experimental dependence  $1/\chi(T)$ , in the temperature range  $100 < T < 273$  K, gives for  $\text{EuErCuSe}_3$  the following Curie-Weiss constant and paramagnetic Curie temperature values:  $C = 0.031 \text{ K cm}^3/\text{g}$ ;  $\Theta = -1 \text{ K}$ , respectively.

Presumably, below the temperature of the magnetic phase transition, the magnetic moments of rare-earth ions  $\text{Eu}^{2+}$  ( $7.94 \mu\text{B}$ ) and  $\text{Er}^{3+}$  ( $9.59 \mu\text{B}$ ) [23,56] form two magnetic sublattices with a mutual antiferromagnetic orientation and uncompensated total magnetic moment. A more accurate picture of the magnetic sublattices behavior can be obtained by neutron diffraction studies.

Temperatures, enthalpies of melting of  $\text{EuLnCuSe}_3$  (Nd, Sm, Gd, Er), were determined by finding of samples in evacuated quartz ampoules, as well as in a graphite crucible (Er) (Figures 7–9, Tables 4 and 5). The thermal stability of the compounds increases markedly, depending on  $r\text{Ln}^{3+}$  (Figure 9).  $\text{EuNdCuSe}_3$  decomposes by a solid-phase reaction (Figure 7a). The state of the sample after DSC has not changed. The thermal stability of  $\text{EuSmCuSe}_3$  increases by more than 150 K, which already leads to the incongruent melting of the compound (Figure 7b); after DSC, the sample is partially melted. The investigated samples did not show phase transitions when they were in the solid state. The  $\text{EuGdCuSe}_3$  compound has two thermal effects of phase transformations at 1494 and 1530 K (Figure 7c). The  $\text{EuErCuSe}_3$  compound has three endothermic effects on the temperature range 1561–1608 K (Figure 7d,e). Samples of phases heated to 1550 K (Gd) to 1613 K (Er) remained in the polycrystalline state, and no signs of the appearance of a liquid phase were found. Thermal effects are reproduced in heating–cooling cycles. For  $\text{EuErCuSe}_3$ , the values of temperature and enthalpy of the heat effect obtained at different installations practically coincide, as shown in Table 4. As for the shape of the peaks, there are linear sections characteristic of phase transformations that correspond to invariant phase equilibria [55,57]. After cooling, the samples have the same crystal structure as before heat treatment. For the sample of  $\text{EuErCuSe}_3$ , ST  $KZrCuS_3$ , SG  $Cmcm$ ,  $a = 4.057$  (3),  $b = 13.357$  (9), and  $c = 10.463$  (7) Å were determined. All the data obtained indicate that the thermal effects are most likely caused by polymorphic transitions in the compounds. High-temperature modifications were not fixed by quenching. Greek letters indicate the observed modifications of compounds with increasing temperature. Thus, the  $\alpha$ - $\text{EuErCuSe}_3$  modification exists from standard conditions to 1561 K,  $\beta$ - $\text{EuErCuSe}_3$ —from 1561 to 1579 K;  $\gamma$ - $\text{EuErCuSe}_3$ —from 1579 to 1600 K; and  $\delta$ - $\text{EuErCuSe}_3$ —from 1600 K to melting.

$\text{EuGdCuSe}_3$  and  $\text{EuErCuSe}_3$  melt incongruently. Broadened peaks of endothermic effects of melting of the samples were recorded at 1588 K (Gd) and 1664 K (Er) (Figure 7c–e). After cooling, the samples had an oval shape, which indicates a partial transition of the samples into the melt. The character of phase melting was studied in detail, during DSC-TG studies of a sample of  $\text{EuErCuSe}_3$ . The initial  $\text{EuErCuSe}_3$  sample becomes multiphase after cooling. According to XRD data, the following phases were found: 65 mol. %  $\text{EuErCuSe}_3$ , 2 mol. %  $\text{EuSe}$ , 19 mol. %  $\text{Eu}_{1-x-y}\text{Er}_x\text{Cu}_y\text{Se}$ , 8 mol. %  $\text{Cu}_{2-x}\text{Se}$ , and 6 mol. %  $\text{Er}_2\text{Se}_3$ . The results of studying a sample cut after DSC are in complete agreement with the SEM data (Figure 8).

The sample microstructure has a continuous  $\text{EuErCuSe}_3$  phase field, in which isolated regions of several phases are located. The phase composition of the multiphase regions is approximately similar, and one of them is shown in Figure 8. In the  $\text{EuErCuSe}_3$  phase field, oval  $\text{EuSe}$  grains are located, and, at the perimeter of  $\text{EuSe}$  grains, the  $\text{Eu}_{1-x}\text{Er}_x\text{Cu}_y\text{Se}$  solid solution is located. The solid solution contains erbium, but copper is fixed at the trace level. A eutectic is formed between the  $\text{Eu}_{1-x}\text{Er}_x\text{Cu}_y\text{Se}$  solid solution and  $\text{Cu}_{2-x}\text{Se}$ . Separate  $\text{Er}_2\text{Se}_3$  crystals are in contact with the eutectic. The crystallization peak of the

$\text{Eu}_{1-x}\text{Er}_x\text{Cu}_y\text{Se} + \text{Cu}_{2-x}\text{Se}$  eutectic was recorded during the cooling at 1091 K. The formation of primary EuSe crystals allows one to draw up the following incongruent  $\text{EuErCuSe}_3$  melting scheme (1).

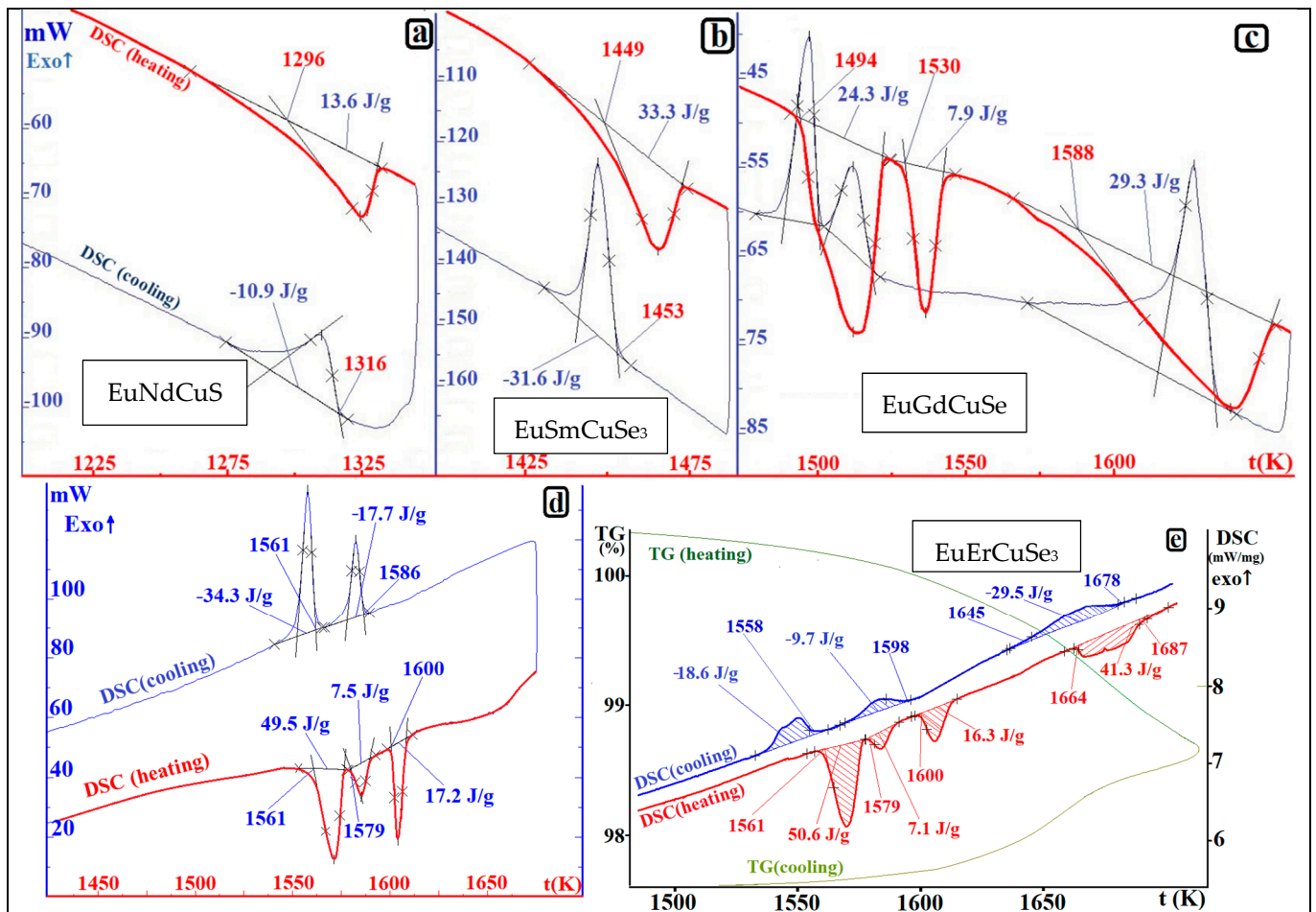
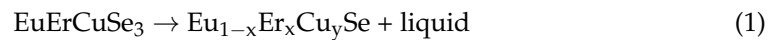


**Figure 7.** Thermograms of  $\text{EuLnCuSe}_3$  (Ln—Nd, Sm, Gd, Er) samples. (a–e)—SC/t dependences of SETARAM SETSYS Evolution for samples (a)— $\text{EuNdCuSe}_3$ , (b)— $\text{EuSmCuSe}_3$ , (c)— $\text{EuGdCuSe}_3$ . (d)— $\text{EuErCuSe}_3$  weighing 40–105 mg, which were in evacuated sealed quartz ampoules. (e)—Netzsch DSC/TG/t dependence of  $\text{EuErCuSe}_3$ , sample weight 76.9 mg, was in an open graphite crucible G-8.

In the temperature range of the endothermic effect at 1664–1687 K, several processes occur simultaneously: the incongruent  $\text{EuErCuSe}_3$  melting, partial thermal dissociation of the compound, and melting of primary crystals of solid solution of the EuSe phase.

From the general peak of the processes  $\Delta H = 41.3 \text{ J/g}$ , an inconsistent melting peak of  $\text{EuErCuSe}_3$  with  $\Delta H = 29 \pm 4 \text{ J/g}$ ,  $18.0 \pm 2.5 \text{ kJ/mol}$  is roughly isolated.

Of particular interest is the comparison of the results, obtained from the thermal analysis of  $\text{EuLnCuSe}_3$  compounds (Table 5) with the thermal properties of related sulfide and selenide compounds (Figure 9). The thermal stability of  $\text{EuLnCuSe}_3$  increases significantly, depending on  $r\text{Ln}^{3+}$ . The enthalpies of incongruent melting of sulfide and selenide quaternary compounds are comparable.

The values of melting points and enthalpies of incongruent decomposition of  $\text{ALnCuX}_3$  ( $A = \text{Eu, Sr, Ba}$ ), ( $X = \text{S, Se}$ ), found in the literature, are presented in Figure 9 [23,58–60].

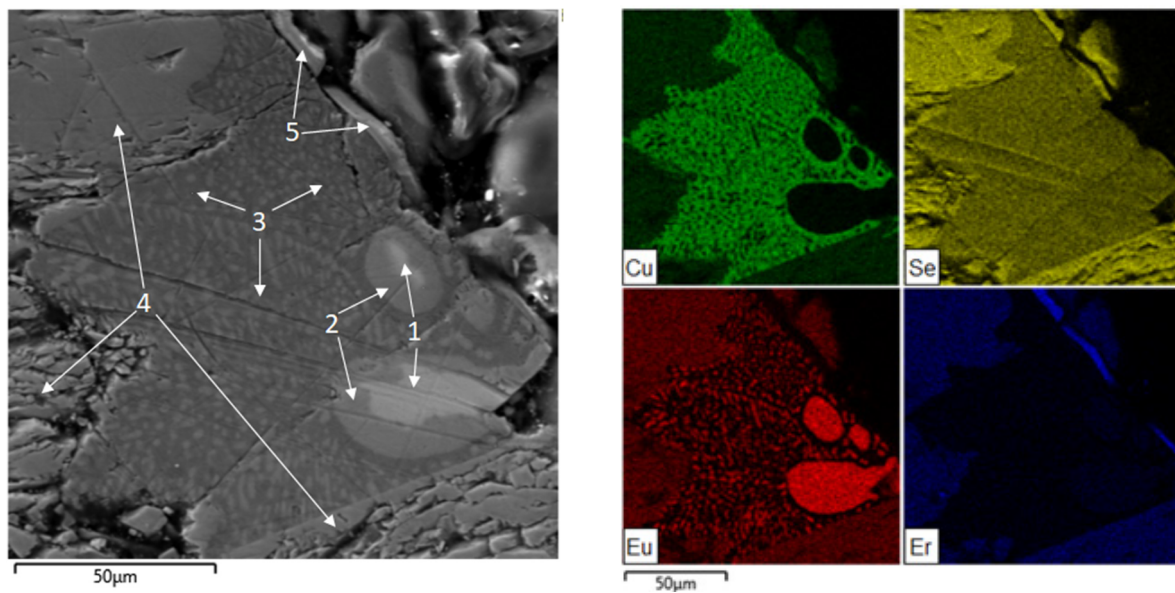


**Figure 8.** SEM/EDS patterns of the sample surface cooled from 1435 °C. Phase designation: 1-EuSe, 2-Eu<sub>1-x-y</sub>Er<sub>x</sub>Cu<sub>y</sub>Se, 3-eutectic formed by phases Eu<sub>1-x</sub>Er<sub>x</sub>Cu<sub>y</sub>Se and Cu<sub>2-x</sub>Se, 4-EuErCuSe<sub>3</sub>, 5-Er<sub>2</sub>Se<sub>3</sub>. Distribution maps of the chemical elements in a EuErCuSe<sub>3</sub> sample cooled after DSC (1708 K).

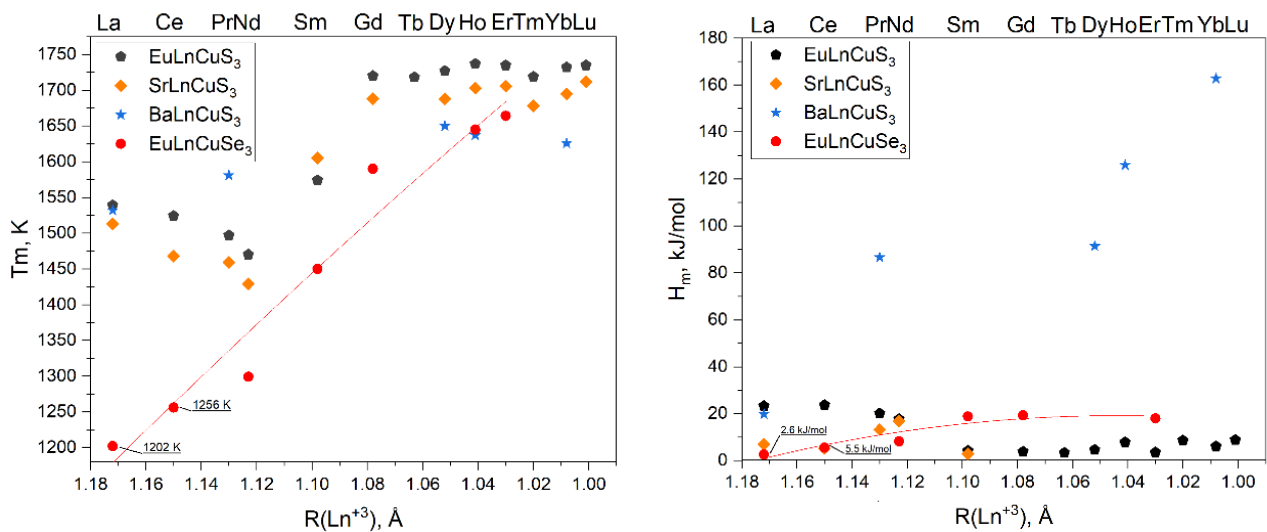


**Figure 9.** Dependences of temperature and (incongruent, congruent) melting enthalpy values of known A LnCuX<sub>3</sub> (A = Eu, Sr, Ba), (X = S, Se) on the ionic radius of Ln<sup>3+</sup> cations.

**Table 4.** Temperature (K) and phase transition enthalpy (kJ mol<sup>-1</sup>) values in the EuErCuSe<sub>3</sub> compound.

NETZSCH Jupiter STA 449 F3					
$T_{\alpha \leftrightarrow \beta}$	$\Delta H_{\alpha \leftrightarrow \beta}$	$T_{\beta \leftrightarrow \gamma}$	$\Delta H_{\beta \leftrightarrow \gamma}$	$T_{\gamma \leftrightarrow \delta}$	$\Delta H_{\gamma \leftrightarrow \delta}$
1561	31.4	1579	4.4	1600	10.1
SETARAM SETSYS Evolution					
1561	30.7	1579	4.6	1600	10.7

**Table 5.** Temperatures and enthalpies of melting of EuLnCuSe<sub>3</sub> compounds.

Compound	Melting Type	$T_{\text{melt}}$ , K	$\Delta H_{\text{melt}}$ , kJ/mol	Compound	Melting Type	$T_{\text{melt}}$ , K	$\Delta H_{\text{melt}}$ , kJ/mol
EuLaCuSe <sub>3</sub>	Solid phase decay	1202	2.6	EuSmCuSe <sub>3</sub>	Incongruent	1449	18.8
EuCeCuSe <sub>3</sub>		1256	5.5	EuGdCuSe <sub>3</sub>		1588	17.9
EuNdCuSe <sub>3</sub>		1296	8.2	EuHoCuSe <sub>3</sub>		1645	-

#### 4. Conclusions

In the series of EuLnCuSe<sub>3</sub> (Ln = Nd, Sm, Gd, Er), regularities are observed that correlate with the electronic structure of rare earth elements and the value of the ionic radius  $r_{\text{Ln}^{3+}}$ . Compounds for the rare earth elements of the first and second tetrads (Nd, Sm, Gd) have SG *Pnma* ST Cu<sub>2</sub>EuSe<sub>3</sub>, for the element of the fourth tetrad (Er), SG *Cmcm* ST KZrCuSe<sub>3</sub> was determined. Depending on the value of the ionic radius  $r_{\text{Ln}^{3+}}$ , the parameters of e.u. and compounds naturally decrease, a trend of increasing microhardness appears, and the thermal stability of compounds significantly increases. The crystal structure of EuErCuSe<sub>3</sub>, established on the isolated single crystal, is crystallochemically similar to the structure of EuErCuSe<sub>3</sub>. Like sulfide compounds, EuErCuSe<sub>3</sub> exhibits a magnetic phase transition  $T_c = 4.7$  K. Below  $T_c$ , the compound is ferromagnetic; above  $T_c$ , it exhibits paramagnetic properties. For EuLnCuSe<sub>3</sub>, depending on the value of the ionic radius  $r_{\text{Ln}^{3+}}$ , the characteristics change naturally: the unit cell parameters naturally decrease, the optical bandgap increases 1.58 eV (Nd), 1.58 eV (Sm), 1.72 eV (Gd), 1.79 eV (Er), the microhardness of the 205 (Nd), 210 (Sm), 225 (Gd) 235 ± 4 HV (Er) phases increases, and the thermal stability of the phases increases significantly. EuNdCuSe<sub>3</sub> decomposes, as a result solid-phase reaction, the rest of the compounds (Sm, Gd, Er) melt incongruently to form a solid solution of EuSe and a liquid phase. EuGdCuSe<sub>3</sub> has two polymorphic transitions, while EuErCuSe<sub>3</sub> has three. Thermal effects of polymorphic transitions are recorded during both heating and cooling. High-temperature modifications of joints are not fixed by quenching.

Further directions in the study of EuLnCuSe<sub>3</sub> should be highlighted. First of all, it is necessary to develop synthesis methods that ensure the preparation of samples without impurity phases. Establish the structures of high-temperature modifications. During the annealing of the samples of compounds at 1270 K, the formation of a selenium phase was observed, which did not cause the appearance of additional impurity phases in the samples. It is possible that the EuLnCuSe<sub>3-x</sub> phases, with vacancies in the structural positions of selenium, will turn out to be more stable. Particles of the EuLnCuSe<sub>3-x</sub> phases have a certain plasticity and are sintered during annealing. The creation of functional ceramics of compounds for studying the spectral characteristics of phases, their certification as new thermoelectrics, and possible components of underwater solar converters is urgent.

**Supplementary Materials:** The following supporting information can be downloaded at: <https://www.mdpi.com/article/10.3390/cryst12010017/s1>. Table S1. Coordinates of atoms in the EuErCuSe<sub>3</sub> compound. Table S2. Bond lengths in EuErCuSe<sub>3</sub> structure.

**Author Contributions:** Conceptualization, O.V.A., Y.G.D. and V.V.A.; methodology, N.N.H.; formal analysis, A.S.A., B.A.Z. and A.P.T.; data curation, D.A.V., D.A.U. and D.D.S.; writing—original draft preparation, N.N.H., O.V.A.; writing—review and editing, Y.G.D.; supervision, O.V.A. All authors have read and agreed to the published version of the manuscript.

**Funding:** The study was funded by the Ministry of Science and Higher Education of the Russian Federation (Projects AAAA-A21-121011390011-4 and AAAA-A19-119031890025-9), as well as the Government of the Tyumen Region (grant to non-profit organizations No. 2. 89-don, dated 7 December 2020).

**Institutional Review Board Statement:** Not applicable.

**Informed Consent Statement:** Not applicable.

**Data Availability Statement:** Not applicable.

**Acknowledgments:** B.A.Z. acknowledge the support by the Ministry of Science and Higher Education of Russia. The work was carried out jointly by Boreskov Institute of Catalysis and Novosibirsk State University. The study was carried out using the equipment of Research and Education Center “Molecular Design and Ecologically Safe Technologies” at the Novosibirsk State University. We would like to express our gratitude to the Tyumen State University Engineering Center for the opportunity to measure microhardness. The authors are grateful to Elena V. Boldyreva and Vladimir V. Boldyrev for their useful pieces of advice, fruitful discussions, and help with manuscript preparation and organizing the XRD studies at the Novosibirsk State University. The XRPD study was carried out at the Institute of Solid State Chemistry, UB RAS.

**Conflicts of Interest:** The authors have no conflict of interest.

## References

1. Christuk, A.E.; Wu, P.; Ibers, J.A. New Quaternary Chalcogenides  $BaLnMQ_3$  (Ln-Rare Earth; M = Cu, Ag; Q = S, Se). *J. Solid State Chem.* **1994**, *110*, 330–336. [[CrossRef](#)]
2. Strobel, S.; Schleid, T. Three structure types for strontium copper(I) lanthanide(III) selenides  $SrCuMSe_3$  (M = La, Gd, Lu). *J. Alloys Compd.* **2006**, *418*, 80–85. [[CrossRef](#)]
3. Gulay, L.D.; Olekseyuk, I.D. Crystal structures of the  $RCuPbSe_3$  (R = Gd, Tb, Dy, Ho, Er, Tm, Yb and Lu) compounds. *J. Alloys Compd.* **2005**, *387*, 160–164. [[CrossRef](#)]
4. Gulay, L.D.; Kaczorowski, D.; Pietraszko, A. Crystal structure and magnetic properties of  $YbCuPbSe_3$ . *J. Alloys Compd.* **2006**, *413*, 26–28. [[CrossRef](#)]
5. Gulay, L.D.; Shemet, V.Y.; Olekseyuk, I.D. Crystal structures of the compounds  $YCuPbSe_3$ ,  $Y_3CuSnSe_7$  and  $Y_3Cu_{0.685}Se_6$ . *J. Alloys Compd.* **2004**, *385*, 160–168. [[CrossRef](#)]
6. Zheng, N.; Bu, X.; Vu, H.; Feng, P. Open-framework chalcogenides as visible-light photocatalysts for hydrogen generation from water. *Angew. Chem. Int. Ed.* **2005**, *44*, 5299–5303. [[CrossRef](#)]
7. Wu, T.; Bu, X.; Feng, P. Three-dimensional open framework built from Cu-S icosahedral clusters and its photocatalytic property. *J. Am. Chem. Soc.* **2008**, *130*, 15238–15239. [[CrossRef](#)]
8. Huang, F.Q.; Mitchell, K.; Ibers, J.A. New layered materials: Syntheses, structures, and optical and magnetic properties of  $CsGdZnSe_3$ ,  $CsZrCuSe_3$ ,  $CsUCuSe_3$ , and  $BaGdCuSe_3$ . *Inorg. Chem.* **2001**, *40*, 5123–5126. [[CrossRef](#)]
9. Gulay, L.D.; Daszkiewicz, M.; Shemet, V.Y.; Pietraszko, A. Crystal structure of the  $R_2PbS_4$  (R = Yb and Lu) compounds. *J. Alloys Compd.* **2008**, *453*, 143–146. [[CrossRef](#)]
10. Liu, Y.; Song, X.-D.; Zhang, R.-C.; Zhou, F.-Y.; Zhang, J.-W.; Jiang, X.-M.; Ji, M.; An, Y.L. Solvothermal syntheses and characterizations of four quaternary copper sulfides  $BaCu_3MS_4$  (M = In, Ga) and  $BaCu_2MS_4$  (M = Sn, Ge). *Inorg. Chem.* **2019**, *58*, 15101–15109. [[CrossRef](#)]
11. Sachanyuk, V.P.; Parasyuk, O.V.; Fedorchuk, A.O.; Atuchin, V.V.; Pervukhina, N.V.; Plotnikov, A.E. The system  $Ag_2Se-Ho_2Se_3$  in the 0–50 mol. %  $Ho_2Se_3$  range and the crystal structure of two polymorphic forms of  $AgHoSe_2$ . *Mater. Res. Bull.* **2007**, *42*, 1091–1098. [[CrossRef](#)]
12. Assoud, A.; Shi, Y.; Guo, Q.; Kleinke, H. Crystal and electronic structure of the new quaternary sulfides  $TlLnAg_2S_3$  (Ln = Nd, Sm and Gd). *J. Solid State Chem.* **2017**, *256*, 6–9. [[CrossRef](#)]
13. Edhaim, F.; Rothenberger, A. Rare Earth chalcogenides  $NaLnSnS_4$  (Ln = Y, Gd, Tb) for selective adsorption of volatile hydrocarbons and gases. *Z. Anorg. Allg. Chem.* **2017**, *643*, 953–961. [[CrossRef](#)]
14. Batouche, M.; Seddik, T.; Ugur, S.; Ugur, G.; Messekine, S.; Vu, T.V.; Khyzhun, O.Y. DFT-investigation on anisotropy degree of electronic, optical, and mechanical properties of olivine  $ZnRE_2S_4$  (RE = Er, Tm) compounds. *Mater. Res. Express* **2020**, *7*, 016305. [[CrossRef](#)]
15. Lin, H.; Chen, H.; Zheng, Y.J.; Chen, Y.-K.; Yu, J.-S.; Wu, L.-M.  $Ba_5Cu_8In_2S_{12}$ : A quaternary semiconductor with a unique 3D copper-rich framework and ultralow thermal conductivity. *Chem. Commun.* **2017**, *53*, 2590–2593. [[CrossRef](#)] [[PubMed](#)]
16. Wakeshima, M.; Furuuchi, F.; Hinatsu, Y. Crystal structures and magnetic properties of novel rare-earth copper sulfides,  $EuRCuS_3$  (R = Y, Gd-Lu). *J. Phys. Condens. Matter* **2004**, *16*, 5503–5518. [[CrossRef](#)]
17. Ruseikina, A.V.; Molokeev, M.S.; Chernyshev, V.A.; Aleksandrovsky, A.S.; Krylov, A.S.; Krylova, S.N.; Velikanov, D.A.; Grigoriev, M.V.; Maximov, N.G.; Shestakov, N.P.; et al. Synthesis, structure, and properties of  $EuScCuS_3$  and  $SrScCuS_3$ . *J. Solid State Chem.* **2021**, *296*, 121926. [[CrossRef](#)]
18. Wu, P.; Christuk, A.E.; Ibers, J.A. New Quaternary Chalcogenides  $BaLnMQ_3$  (Ln = Rare Earth or Sc; M = Cu, Ag; Q = S, Se) II Structure and.pdf. *J. Solid State Chem.* **1994**, *110*, 337–344. [[CrossRef](#)]
19. Yang, Y.; Ibers, J.A. Synthesis and Characterization of a Series of Quaternary Chalcogenides  $BaLnMQ_3$  (Ln = Rare Earth, M = Coinage Metal, Q = Se or Te). *J. Solid State Chem.* **1999**, *147*, 366–371. [[CrossRef](#)]

20. Strobel, S.; Schleid, T. Quaternary strontium copper(I) lanthanoid(III) selenides with cerium and praseodymium: SrCuCeSe<sub>3</sub> and SrCuPrSe<sub>3</sub>, unequal brother and sister. *Z. Naturforsch.-Sect. B J. Chem. Sci.* **2004**, *59*, 985–991. [[CrossRef](#)]
21. Mansuetto, M.F.; Keane, P.M.; Ibers, A.J. Synthesis, Structure, and Conductivity of the New Group IV Chalcogenides, KCuZrQ<sub>3</sub> (Q = S, Se, Te). *J. Solid State Chem.* **1992**, *101*, 257–264. [[CrossRef](#)]
22. Ruseikina, A.V.; Solovyov, L.A.; Chernyshev, V.; Aleksandrovsky, A.S.; Andreev, O.V.; Krylova, S.N.; Krylov, A.S.; Velikanov, D.A.; Molokeev, M.S.; Maximov, N.G.; et al. Synthesis, structure, and properties of EuErCuS<sub>3</sub>. *J. Alloys Compd.* **2019**, *805*, 779–788. [[CrossRef](#)]
23. Ruseikina, A.V.; Chernyshev, V.A.; Velikanov, D.A.; Aleksandrovsky, A.S.; Shestakov, N.P.; Molokeev, M.S.; Grigoriev, M.V.; Andreev, O.V.; Garmonov, A.A.; Matigorov, A.V.; et al. Regularities of the property changes in the compounds EuLnCuS<sub>3</sub> (Ln = La–Lu). *J. Alloys Compd.* **2021**, *874*, 159968. [[CrossRef](#)]
24. Sokolov, V.V.; Kamarzin, A.A.; Trushnikova, L.N.; Savelyeva, M.V. Optical Materials Containing Rare Earth Ln<sub>2</sub>S<sub>3</sub> Sulfides. *J. Alloys Compd.* **1995**, *225*, 567–570. [[CrossRef](#)]
25. Reed, T.B.; Fahey, R.E.; Strauss, A.J. Sealed crucible technique for thermal analysis of volatile compounds up to 2500 °C: Melting points of EuO, EuS, EuSe and EuTe. *J. Cryst. Growth* **1972**, *15*, 174–178. [[CrossRef](#)]
26. Fang, C.M.; Meetsma, A.; Wieggers, G.A. Crystal structure of erbium sesquiselenide, Er<sub>2</sub>Se<sub>3</sub>. *J. Alloys Compd.* **1995**, *218*, 224–227. [[CrossRef](#)]
27. Fainberg, N.Y.; Andreev, O.V.; Kharitontsev, V.B.; Polkovnikov, A.A. Sm–Sm<sub>2</sub>Se<sub>3</sub> phase diagram and properties of phases. *Russ. J. Inorg. Chem.* **2016**, *61*, 93–98. [[CrossRef](#)]
28. Pribyl'skii, N.Y.; Vasilieva, I.G.; Gamidov, R.S. Phase equilibria of the Gd–Se system. *Mater. Res. Bull.* **1982**, *17*, 1147–1153. [[CrossRef](#)]
29. Bagieva, M.R.; Aliev, I.I.; Babanly, M.B. Phase relations in the SnSe<sub>2</sub>–Er<sub>2</sub>Se<sub>3</sub> system. *Inorg. Mater.* **2003**, *39*, 927–930. [[CrossRef](#)]
30. Parasyuk, O.V.; Atuchin, V.V.; Romanyuk, Y.E.; Marushko, L.P.; Piskach, L.V.; Olekseyuk, I.D.; Volkov, S.V.; Pekhnyo, V.I. The CuGaSe<sub>2</sub>–CuInSe<sub>2</sub>–2CdS system and single crystal growth of the g-phase. *J. Cryst. Growth*, 2011; *318*, 332–336. [[CrossRef](#)]
31. Kokh, K.A.; Atuchin, V.V.; Adichtchev, S.V.; Gavrilova, T.A.; Bahadur, A.M.; Klimov, A.S.; Korolkov, I.V.; Kuratieva, N.; Mukherjee, S.; Pervukhina, N.V.; et al. Cu<sub>2</sub>ZnSnS<sub>4</sub> crystal growth using an SnCl<sub>2</sub> based flux. *Cryst. Eng. Comm.* **2021**, *23*, 1025–1032. [[CrossRef](#)]
32. Murray, R.M.; Heyding, R.D. The Copper–Selenium System at Temperatures to 850 K and Pressures to 50 Kbar. *Can. J. Chem.* **1975**, *53*, 878–887. [[CrossRef](#)]
33. Chakrabarti, D.J.; Laughlin, D.E. The Cu–Se (Copper–Selenium) system. *Bull. Alloy Phase Diagrams* **1981**, *2*, 305–315. [[CrossRef](#)]
34. Eick, H.A. The crystal structure and lattice parameters of some rare earth mono-seleno oxides. *Acta Crystallogr.* **1960**, *13*, 161. [[CrossRef](#)]
35. Christensen, A.N. Investigation by the use of profile refinement of neutron powder diffraction data of the geometry of the (Si<sub>2</sub>O<sub>7</sub>)<sup>6-</sup> ions in the high temperature phases of rare earth disilicates prepared from the melt in crucible-free synthesis. *Z. Krist.* **1994**, *209*, 7–13. [[CrossRef](#)]
36. Antipov, E.; Putilin, S.; Shpanchenko, R. *ICDD Grant-in-Aid*; Moscow State University: Moscow, Russia, 1994.
37. Souleau, C.; Guittard, M. Sur les systmes forms entre les sliures L<sub>2</sub>Se<sub>3</sub> des lments des terres rares et le sliure EuSe d'euporium. *Bull. Soc. Chim.* **1968**, *1968*, 3632.
38. Zhu, W.J.; Huang, Y.Z.; Dong, C.; Zhao, Z.X. Synthesis and crystal structure of new rare-earth copper oxyselenides: R Cu Se O (R = La, Sm, Gd and Y). *Mater. Res. Bull.* **1994**, *29*, 143. [[CrossRef](#)]
39. Kojima, K.; Nishizawa, S.; Hiraoka, K.; Hihara, T.; Kamigaichi, T. Valence change of Sm ion in Eu<sub>1-x</sub>Sm<sub>x</sub>Se. *Solid State Commun.* **1983**, *46*, 417. [[CrossRef](#)]
40. Berdonosov, P.S.; Kusainova, A.M.; Kholodkovskaya, L.N.; Dolgikh, V.A.; Akselrud, L.G.; Popovkin, B.A. Powder X ray and IR studies of the new oxyselenides M O Cu Se (M = Bi, Gd, Dy). *J. Solid State Chem.* **1995**, *118*, 74. [[CrossRef](#)]
41. Toby, B.H. EXPGUI, a graphical user interface for GSAS. *J. Appl. Crystallogr.* **2001**, *34*, 210–213. [[CrossRef](#)]
42. Larson, A.C.; von Dreele, R.B. *General Structure Analysis System (GSAS)*; Los Alamos National Laboratory Report LAUR; APS, Aragon National Laboratory: Chicago, IL, USA, 2004; pp. 86–748.
43. STOE & Cie. X-Area; STOE & Cie GmbH: Darmstadt, Germany, 2013.
44. Rigaku, O.D. *CrysAlis PRO*; Rigaku Oxford Diffraction Ltd.: Yarnton, UK, 2019.
45. Sheldrick, G.M. SHELXT—Integrated space-group and crystal-structure determination. *Acta Crystallogr. Sect. A* **2015**, *71*, 3–8. [[CrossRef](#)] [[PubMed](#)]
46. Sheldrick, G.M. Crystal structure refinement with SHELXL. *Acta Crystallogr. Sect. C* **2015**, *71*, 3–8. [[CrossRef](#)]
47. Hübschle, C.B.; Sheldrick, G.M.; Dittrich, B. ShelXle: A Qt graphical user interface for SHELXL. *J. Appl. Crystallogr.* **2011**, *44*, 1281–1284. [[CrossRef](#)]
48. Joint CCDC/FIZ Karlsruhe Online Deposition Service. Available online: <https://www.ccdc.cam.ac.uk/structures/> (accessed on 21 December 2021).
49. Velikanov, D.A. Vibration Magnetic Meter. RF Patent for the Invention RU2341810 (C1). Publ. 20.12.2008, Bulletin No. 35. Available online: <https://worldwide.espacenet.com/patent/search?q=RU2341810> (accessed on 21 December 2021).
50. Puzey, I.M.; Sabinin, P.G. Electromagnet for physico-chemical studies. *Prib. Tekh. Eksp.* **1960**, *1*, 104–109.

51. Velikanov, D.A. High-sensitivity measurements of the magnetic properties of materials at cryogenic temperatures. *Inorg. Mater. Appl. Res.* **2020**, *11*, 801–808. [[CrossRef](#)]
52. Velikanov, D.A. Magnetometer with a Superconducting Quantum Interferometric Sensor. RF Patent for the Invention RU2481591 (C1). Publ. 10.05.2013, Bulletin No. 13. Available online: <https://worldwide.espacenet.com/patent/search?q=RU2481591> (accessed on 21 December 2021).
53. NETZSCH Proteus 6. *Thermic Analyses—User's and Software Manuals*; Netzsch-Gerätebau: Selb, Germany, 2012.
54. Shannon, R.D. Revised Effective Ionic Radii and Systematic Studies of Interatomic Distances in Halides and Chalcogenides. *Acta Cryst.* **1976**, *A32*, 751–767. [[CrossRef](#)]
55. Andreev, P.O.; Polkovnikov, A.A.; Denisenko, Y.G.; Andreev, O.V.; Burkhanova, T.M.; Bobylev, A.N.; Pimneva, L.A. Temperatures and enthalpies of melting of Ln<sub>2</sub>S<sub>3</sub> (Ln = Gd, Tb, Dy, Ho, Er, Tm, Yb, and Lu) compounds. *J. Therm. Anal. Calorim.* **2018**, *131*, 1545–1551. [[CrossRef](#)]
56. van den Eeckhout, K.; Smet, P.F.; Poelman, D. Persistent luminescence in Eu<sup>2+</sup>-doped compounds: A review. *Materials* **2010**, *3*, 2536–2566. [[CrossRef](#)]
57. Ruseikina, A.V.; Andreev, O.V.; Galenko, E.O.; Koltsov, S.I. Trends in thermodynamic parameters of phase transitions of lanthanide sulfides SrLnCuS<sub>3</sub> (Ln = La – Lu). *J. Therm. Anal. Calorim.* **2017**, *128*, 993–999. [[CrossRef](#)]
58. Azarapin, N.O.; Aleksandrovsky, A.S.; Atuchin, V.V.; Gavrilova, T.A.; Krylov, A.S.; Molokeev, M.S.; Mukherjee, S.; Oreshonkov, A.S.; Andreev, O.V. Synthesis, structural and spectroscopic properties of orthorhombic compounds BaLnCuS<sub>3</sub> (Ln = Pr, Sm). *J. Alloys Compd.* **2020**, *832*, 153134. [[CrossRef](#)]
59. Azarapin, N.O.; Atuchin, V.V.; Maximov, N.G.; Aleksandrovsky, A.S.; Molokeev, M.S.; Oreshonkov, A.S.; Shestakov, N.P.; Krylov, A.S.; Burkhanova, T.M.; Mukherjee, S.; et al. Synthesis, structure, melting and optical properties of three complex orthorhombic sulfides BaDyCuS<sub>3</sub>, BaHoCuS<sub>3</sub> and BaYbCuS<sub>3</sub>. *Mater. Res. Bull.* **2021**, *140*, 111314. [[CrossRef](#)]
60. Oreshonkov, A.S.; Azarapin, N.O.; Shestakov, N.P.; Adichtchev, S.V. Experimental and DFT study of BaLaCuS<sub>3</sub>: Direct band gap semiconductor. *J. Phys. Chem. Solids* **2021**, *148*, 109670. [[CrossRef](#)]